Notch-dependent repression of miR-155 in the bone marrow niche regulates hematopoiesis in an NF-κB dependent manner

Lin Wang[1], **Huajia Zhang**[1], **Sonia Rodriguez**[1], **Liyun Cao**[1], **Jonathan Parish**[1], **Christen Mumaw**[1], **Amy Zollman**[1], **Gosia Kamocka**[2], **Jian Mu**[3], **Danny Z. Chen**[3], **Edward F. Srour**[1,2], **Brahmananda R. Chitteti**[2], **Harm HogenEsch**[4], **Xiaolin Tu**[5], **Teresita M. Bellido**[5], **Scott Boswell**[2], **Taghi Manshouri**[6], **Srdan Verstovsek**[6], **Mervin C. Yoder**[1], **Reuben Kapur**[1], **Angelo A. Cardoso**[1], and **Nadia Carlesso**[1,*]

[1]Wells Center for Pediatric Research, Department of Pediatrics, Indiana University School of Medicine, Indianapolis, IN, 46202, USA

[2]Department of Medicine, Indiana University School of Medicine, Indianapolis, IN, 46202, USA

[3]Department of Computer Science and Engineering, University of Notre Dame, South Bend, IN, 46556, USA

[4]Department of Comparative Pathobiology, College of Veterinary Medicine, Purdue University, West Lafayette, IN 47907, USA

[5]Department of Anatomy and Cell Biology, Indiana University School of Medicine, Indianapolis, IN, 46202, USA

[6]Leukemia Department, MD Anderson Cancer Center, Houston, TX, USA

Summary

MicroRNA (miR)-155 has been implicated in regulating inflammatory responses and tumorigenesis, but its precise role in linking inflammation and cancer has remained elusive. Here, we identify a connection between miR-155 and Notch signaling in this context. Loss of Notch signaling in the bone marrow (BM) niche alters hematopoietic homeostasis and leads to lethal myeloproliferative-like disease. Mechanistically, Notch signaling represses miR-155 expression by promoting binding of RBPJ to the miR-155 promoter. Loss of Notch/RBPJ-signaling upregulates miR-155 in BM endothelial cells, leading to miR-155-mediated targeting of the NF-κB inhibitor κB-Ras1, NF-κB activation and increased proinflammatory cytokine production. Deletion of miR-155 in the stroma of RBPJ^{-/-} mice prevented the development of myeloproliferative-like disease and cytokine induction. Analysis of BM from patients carrying

---

*Correspondence to: Nadia Carlesso, M.D., Ph.D. Herman B Wells Center for Pediatric Research, Indiana University School of Medicine, 1044 W. Walnut, Bldg. R4-Room 166, Indianapolis, IN 46202, Ph: 317-274-2134, ncarless@iu.edu.

None of the authors of this manuscript has any financial conflict of interest that might be construed to influence the results or interpretation of the results reported in this communication.

Publisher's Disclaimer: This is a PDF file of an unedited manuscript that has been accepted for publication. As a service to our customers we are providing this early version of the manuscript. The manuscript will undergo copyediting, typesetting, and review of the resulting proof before it is published in its final citable form. Please note that during the production process errors may be discovered which could affect the content, and all legal disclaimers that apply to the journal pertain.

myeloproliferative neoplasia also revealed elevated expression of miR-155. Thus, the Notch/miR155/kB-Ras1/NF-kB axis regulates the inflammatory state of the BM niche and affects the development of myeloproliferative disorders.

Introduction

Notch signaling plays an essential role in regulating normal and abnormal hematopoietic stem and progenitor cell development and functions. While Notch's cell-autonomous role in this process is well established, its non-cell autonomous role remains poorly understood. Specifically, the cellular and molecular mechanism(s) by which Notch loss-of-function regulates the integrity of the BM niche is poorly defined. Here, we used a conditional knock-out model of RBPJ, a non-redundant downstream effector of the canonical Notch signaling cascade, to determine the contribution of Notch signaling to the non-cell autonomous regulation of hematopoiesis.

Notch genes encode large, highly conserved type 1 transmembrane receptors, which are activated through cell-cell contact by binding to one of their ligands on neighboring cells (Artavanis-Tsakonas et al., 1999). Notch binding and activation is regulated at multiple steps by molecules that control endocytosis, O-fucosylation and proteolytic cleavage, leading to the release of the Notch intracellular domain (NICD) and its translocation to the nucleus (De Strooper et al., 1999). Following ligand activation, Notch signalling can be distinguished into canonical and non-canonical pathways on the basis of whether NICD interacts with a CSL transcription factor (CBF1/RBP-J, Su(H), Lag-1) (Kopan and Ilagan, 2009). In mice, the CSL factor is known as RBPJk (recombination signal binding protein for immunoglobulin kappa J region) and functions as a transcriptional repressor. Canonical Notch signalling involves NICD binding to RBPJ and converting it from a repressor to an activator, resulting in the transcription of Notch-dependent genes which can influence the developmental and differentiation programs (Davis and Turner, 2001). Evidences of NICD binding to RBPJ maintaining a repressor status have been recently reported and involve dislocation and recruitment of co-activators and co-repressors, respectively (Sakano et al., 2010; Tiberi et al., 2012).

Although the precise mechanism(s) involved in the regulation of hematopoiesis via the non-cell-autonomous Notch signaling cascade remain unclear, recent studies have begun to shed some insight into this process (Kim et al., 2008; Yao et al., 2011; Yoda et al., 2011, Klinakis et al, 2011). While informative, the genetic models used in these studies involved deletion of genes that affect global Notch signaling, both CSL-dependent and CSL-independent Notch signaling, and regulate other molecules/effectors in addition to Notch (Pruessmeyer and Ludwig, 2009;De Strooper, 2005), thus, preventing a clear understanding of the specific downstream mechanisms.

In this study, we show that RBPJ functions as a transcriptional repressor on the promoter of the microRNA miR-155. miR-155 is encoded from the B cell integration cluster locus and is upregulated in cancer and in inflammation (Tili et al., 2013). Loss of canonical Notch signaling induces direct upregulation of miR-155 expression on BM stromal and endothelial cells and causes significant alterations of hematopoiesis. Constitutive miR-155 up-regulation

due to loss of RBPJ transcriptional repression induces NF-κB activation and a global state of inflammation in the BM niche, leading to an uncontrolled expansion of myeloid cells and to the development of a myeloproliferative-like disease. Our results demonstrate a connection between Notch signaling, miR-155 and NF-κB and suggest a critical role for this pathway in maintaining hematopoietic homeostasis and linking inflammation and cancer.

Results

RBPJ deletion in the BM microenvironment disrupts hematopoietic homeostasis and induces a non-cell autonomous myeloproliferative-like disease

Inhibition of RBPJ transcriptional activity by deletion of its DNA binding motif results in the complete loss of signaling via all Notch receptors (Han et al., 2002). This RBPJ knock-out model has been successfully used to unveil the role of Notch in the lymphoid compartment; however, the effects of RBPJ deletion on myeloid cells were not investigated. RBPJ was conditionally deleted in the hematopoietic system by injecting mice with pIpC, which induces *MX1-Cre* expression in hematopoietic (CD45$^+$) as well as in stromal cells (CD45$^-$) of the BM (Figure S1A-B). Analysis of stem and progenitor pools within the BM, spleen and peripheral blood (PB) of mice lacking RBPJ revealed a significant increase in the frequency and absolute number of phenotypically defined primitive lineage negative Kit$^+$ Sca-1$^+$ (LSK) cells, including long-term HSCs (LT-HSC), of common myeloid progenitors (CMP) and of granulocyte-macrophage progenitors (GMP; Figure 1A, D and S1C-F). These increases were reflected as expansion of immature myeloid (Gr1$^-$Mac1$^+$ cells) and neutrophils in the BM, spleen and PB of *RBPJ$^{-/-}$* mice relative to controls (Figure 1G-H, left panels and Fig.7G). The number of megakaryocyteerythroid progenitors (MEP), red blood cells (RBC), hemoglobin (Hb), hematocrit (HCT) and platelets (PLT) were reduced in mice lacking RBPJ (Figure S1G, Q). *RBPJ$^{-/-}$* mice developed significant splenomegaly (Figure 1C) and histologic analysis confirmed myeloid expansion in the BM and spleen, and myeloid cell infiltrates in liver and other parenchymal organs. Overall, BM cellularity was significantly increased (Figure S1H). Leukocyte counts and differentials showed a progressive increase of myeloid cells in the PB of RBPJ$^{-/-}$ mice compared to controls: from 2 fold increase at week 4, to 7 fold at week 20 after pIpC (Figure 1H and S1N-O). As reported in a previous study (Han et al., 2002), loss of Notch signaling in the lymphoid compartment was characterized by reduction of T-cells and relative expansion of B-cells (Figure S1P, left graph). Interestingly, B-cells were increased in the PB, but not in the BM and spleen of RBPJ-/- mice (data not shown). *RBPJ$^{-/-}$* mice failed to live past 27 weeks and died of a myeloproliferative disease (Fig. 1I). In contrast, mice haplo-insufficient for *RBPJ$^{+/-}$* did not develop disease, showing comparable survival to control animals up to 40 weeks of follow-up.

To assess the relative contribution of cell-autonomous and non-cell-autonomous mechanisms, we performed reciprocal transplantation studies. BM cells from *RBPJ$^{+/+}$* and *RBPJ$^{-/-}$* expressing the CD45.2 allele were transplanted into wild-type (WT) mice expressing the CD45.1 allele. Similarly to the *RBPJ$^{-/-}$* mice, the LSK pool was significantly increased in WT mice reconstituted with *RBPJ$^{-/-}$* donor cells compared to controls (Figure 1B, left side). However, there was no difference in the representation of GMP, CMP and

MEP subsets in $RBPJ^{-/-}$ and $RBPJ^{+/+}$ donor populations (Figure 1E and S1I). Mice reconstituted with $RBPJ^{-/-}$ donor cells did not show myeloid cell expansion and exhibited normal levels of $Gr1^{+}Mac1^{+}$ neutrophils in the BM, SP and PB (Figure 1G-H, center panels). These mice did not display alterations in RBC, Hb, HCT or PLT (Figure S1Q), nor did they develop splenomegaly, and their survival was similar to the control cohort (Figure 1I). As previously reported, mice reconstituted with $RBPJ^{-/-}$ donor cells presented an overall decrease in T-cells accompanied by a relative increase in B-cells (data not shown). The leukocyte differential count in the recipients of $RBPJ^{-/-}$ donor cells did not show neutrophilia or lymphocytosis (Figure S1N), indicating that the effects observed in $RBPJ^{-/-}$ mice were not solely mediated by a cell-autonomous mechanism.

To examine the contribution of the microenvironment to the myeloproliferative-like disease, we transplanted WT BM cells into $RBPJ^{-/-}$ or $RBPJ^{+/+}$ recipients. Comparative analysis of hematopoietic subsets in the BM and spleen of $RBPJ^{-/-}$ recipients revealed that the loss of $RBPJ$ in the BM microenvironment had a lower impact on the LSK pool in $RBPJ^{-/-}$ recipients (Figures 1B, right side and S1J) than in parental $RBPJ^{-/-}$ mice or WT mice transplanted with $RBPJ^{-/-}$ cells, demonstrating a cell-autonomous contribution of RBPJ on HSC homeostasis. However, similar to the $RBPJ^{-/-}$ parental animals, $RBPJ^{-/-}$ recipient mice transplanted with WT cells showed a significant increase in the frequencies and absolute numbers of CMP and GMP, in both BM and spleen (Figure 1F and S1L). These changes were associated with a marked decrease of MEP, RBC, Hb, and HCT (Figure S1K, Q), and a significant increase in circulating LSK cells (Figure S1J). $RBPJ^{-/-}$ recipients showed a rapid and progressive increase in neutrophils and $Gr1^{+}/Mac1^{+}$ cells in the PB, spleen and BM (Figure 1G-H, right panel) as well as increased BM cellularity (Figure S1M). $RBPJ^{-/-}$ recipients developed marked splenomegaly (Figure 1C, 7D), hypercellular BM with myeloid cell expansion and myeloid infiltrates in the parenchymal organs (data not shown). A complete leukocyte count and differential in the PB of $RBPJ^{-/-}$ recipients indicated a significant increase of myeloid cells (3 fold) compared to $RBPJ^{+/+}$ recipients, whereas lymphoid cells showed a kinetic of engraftment similar to the controls, and a relative decrease in frequency in favor of myeloid cells (Figure 1SN-P). Thus, the loss of $RBPJ$ in the microenvironment resulted in a lethal myeloproliferative-like disease, which evolved rapidly following BM transplant, as indicated by the shorter survival of $RBPJ^{-/-}$ recipients compared to $RBPJ^{-/-}$ mice (100% of the mice were dead by week 10; Figure 1I).

These data demonstrate that loss of Notch/RBPJ canonical pathway is not sufficient to induce a cell-autonomous myeloid disease. Furthermore, they clearly show that loss of RBPJ in the microenvironment is necessary and sufficient to induce a lethal myeloproliferative-like disease in a non-cell autonomous manner.

RBPJ deficiency in the BM niche favors myeloid cell expansion and mobilization by upregulating expression of G-CSF

Given that *Mx1-Cre* is expressed in the stromal cells of multiple organs (Schneider et al., 2003), we questioned whether the BM microenvironment was a critical site for disease initiation of $RBPJ^{-/-}$ mice. $RBPJ^{-/-}$ and $RBPJ^{+/+}$ littermates were transplanted with equal number of BM cells harvested from *Lys-EGFP* reporter mice (wild-type *RBPJ*), in which

EGFP expression is driven by the lysozyme promoter (Faust et al., 2000). As lysozyme expression is specific to myeloid cells (Miyamoto et al., 2002), this strategy provided optimal visualization of the myeloid compartment by intravital fluorescent microscopy (IVFM). The BM niche was imaged at 24 hours and at weeks 2, 4 and 6 after transplantation (Figure 2A). Homing at 24 hours was similar in both conditions; however, by week 2, Lys-EGFP cells transplanted in $RBPJ^{-/-}$ recipients had underwent a more rapid and robust expansion then Lys-EGFP cells transplanted in $RBPJ^{+/+}$ mice (Figure 2A-B). At weeks 4 and 6 after transplantation, the content of Lys-EGFP cells in the BM of $RBPJ^{-/-}$ recipients remained higher but not substantially different from $RBPJ^{+/+}$ recipients, as Lys-EGFP cells had also expanded in the $RBPJ^{+/+}$ recipients (Figure 2B). However, in $RBPJ^{-/-}$ recipients the Lys-EGFP cell expansion in the BM was associated with a greater output of neutrophils and $Gr1^+/Mac1^+$ cells in the PB and progressive enlargement of the spleen (Figure 2D-E). Significant increase in the proportion of myeloid cells in the BM of $RBPJ^{-/-}$ recipients was observed again at advanced stages of disease (Figure 1G).

Lys-EGFP is increasingly expressed from CMP to GMP to mature neutrophils, allowing measurement of the kinetics of differentiation by fluorescent intensity. As expected, Lys-EGFP expression was low in LSK cells in both groups, while analysis of CMP and GMP revealed a higher number of high Lys-EGFP expressing cells in $RBPJ^{-/-}$ recipients than in $RBPJ^{+/+}$ recipients, suggesting a more rapid rate of myeloid cell differentiation (Figure 2C). These data indicate that the $RBPJ^{-/-}$ BM microenvironment is a primary site of myeloid cell expansion, which is accompanied by rapid differentiation and mobilization of myeloid cells in the PB and spleen.

Analysis of serum cytokines by cytokine arrays revealed a significant increase in the levels of several inflammatory cytokines in $RBPJ^{-/-}$ mice (Figure S2A), in particular G-CSF, a driver of myeloid cell proliferation and differentiation. Increased G-CSF levels were confirmed in the BM milieu and in the serum of $RBPJ^{-/-}$ mice by ELISA (Figure 3A-B). Heterozygous $RBPJ^{+/-}$ mice, which did not develop disease, displayed G-CSF levels just above the baseline of normal mice. To determine the contribution of G-CSF to the myeloproliferative-like disease, we treated $RBPJ^{-/-}$ mice with anti-G-CSF neutralizing antibodies. Anti-G-CSF treatment resulted in the normalization of $Gr1^+/Mac1^+$ cells in the PB (Figure 3C), in a significant reduction in the spleen size (Figure 3D), a notable decrease in the proportion of CMPs and a significant reduction in level of GMPs (Figure 3E). These data suggest that G-CSF is a major but not the sole contributor to the myeloproliferative-like disease occurring in $RBPJ^{-/-}$ mice. TNFα levels were also consistently elevated in the absence of RBPJ (Figure S2A-C), suggesting that TNFα, a cytokine involved in myeloid progenitor homeostasis (Walkley et al., 2007), may play a synergistic role with G-CSF in promoting myeloid cell expansion.

Analysis of cytokines in the supernatant of $RBPJ^{-/-}$ BM-derived stromal cells, validated for loss of RBPJ and Notch signaling (Figure 3F-G), demonstrated a pro-inflammatory profile similar to the one observed in the serum (Figure S2B). These experiments confirmed a significant increase in the levels of G-CSF and TNFα in $RBPJ^{-/-}$ stromal cells (Figure 3H). Accordingly, $RBPJ^{-/-}$ BM-derived stromal cells showed a greater ability to support myeloid cell expansion and differentiation of BM Lin⁻ progenitors in co-culture experiments (Figure

3I). These results demonstrate that RBPJ deletion in the BM stromal cells induces pro-inflammatory cytokines, generating a BM niche exceedingly favorable to myeloid progenitor cell expansion.

Contribution of *RBPJ*$^{-/-}$ BM endothelial cells to the myeloproliferative-like disease

Next, we sought to determine which specific stromal cell type(s) in the BM were responsible for the increased cytokine production in RBPJ deficient mice. Co-culture experiments of Lin$^-$ progenitor cells with *RBPJ*$^{-/-}$ derived osteoblasts (OB) or characterization of hematopoiesis in mice with RBPJ deletion in osteocytes did not show impact on the myeloid compartment, ruling out a major role of mature bone cells in the myeloid expansion (Figure S3A-E). In contrast, sorted BM CD45$^-$CD105$^+$CD31$^-$ cells (enriched in mesenchymal like-cells; BM MSC) and BM CD45$^-$CD105$^+$CD31$^+$ VE-cadherin$^+$ cells (enriched in endothelial cells; BM EC) demonstrated higher levels of *G-CSF* and *TNFα* in association with RBPJ deletion (Figure 4A-C). Given the significantly higher expression of *G-CSF* and *TNFα* in BM ECs of *RBPJ*$^{-/-}$ mice and the known role these cells play in producing pro-inflammatory cytokines, we sought to further investigate the role of the BM endothelial niche. To this end, we crossed *RBPJ*$^{-/-}$ mice with the tamoxifen-inducible *Tie2Cre*^{ER} mice. In these mice, the Cre recombinase is expressed under the control of the *Tie2* promoter in which specific regulatory elements were modified to restrict the expression of Cre to ECs, with negligible expression in the hematopoietic system (Forde et al., 2002). Tamoxifen-induced *Tie2CreER*$^+$/*RBPJ*$^{lox/lox}$ and *Tie2CreER*$^-$/*RBPJ*$^{lox/lox}$ mice (referred as *Tie2RBPJ*$^{-/-}$ and *Tie2RBPJ*$^{+/+}$ mice) were analyzed at 6 months post-induction. In these mice, the average reduction of *RBPJ* on sorted BM EC was approximately 30%. Despite the incomplete deletion of EC RBPJ, analysis of the hematopoietic compartment of *Tie2RBPJ*$^{-/-}$ mice demonstrated a significant increase in neutrophils and Gr1$^+$/Mac1$^+$ cells in the PB (Figure 4D-E), increased Gr1$^+$/Mac1$^+$, CMP and GMPs cells in the spleen (Figure 4F-G) and splenomegaly (Figure 4H) compared to *Tie2RBPJ*$^{+/+}$ mice. These changes were associated with increased levels of G-CSF and TNFα in *Tie2RBPJ*$^{-/-}$ mice serum (Figure 4I). All parameters of myeloid cell expansion were similarly increased in *Tie2RBPJ*$^{-/-}$ mice as those observed in *Mx1RBPJ*$^{-/-}$ mice (i.e. CMP and GMP; Figure 4G); however these changes occurred less rapidly in the *Tie2RBPJ*$^{-/-}$ background. Thus, deletion of *RBPJ* in ECs is sufficient to induce myeloid cell expansion. However, the contribution of other stromal cell types, including MSCs, may be important for the development of a full blown and rapid myeloproliferative-like disease.

Loss of RBPJ transcriptional repression induces up-regulation of miR-155

The coordinated upregulation of multiple inflammatory cytokines upon deletion of *RBPJ* suggests the involvement of master regulators triggering a proinflammatory circuitry. Likely candidates for such function are microRNAs. Analysis of the expression of several microRNAs implicated in inflammation showed a significant increase in the expression of *miR-155* in *RBPJ*$^{-/-}$ BM stromal cells (Figure 5A). No significant changes in the expression of *miR-196b, miR-210, miR-125a* and *miR-146a* were noted under similar conditions (Figure S4A). Increased expression of *miR-155* in *RBPJ*$^{-/-}$ stroma was further validated using BM sorted populations enriched in MSCs and ECs, as well as in ECs derived from *Tie2RBPJ*$^{-/-}$ mice (Figure 5B). *miR-155* expression was also up-regulated in Lin$^-$ *RBPJ*$^{-/-}$ hematopoietic

cells, but not in bulk CD45$^+$ cells (Figure S4B and S5D). To determine the molecular link between *RBPJ* and *miR-155* in vitro, murine microvascular endothelial cells (here indicated as EC) and BM stromal cell lines Raw264.7 (Raw) and OP9, were transfected with shRNAs directed towards RBPJ (*shRBPJ*) (Figure S4C). Expression of the *shRBPJ* upregulated *miR-155* expression in ECs, Raw cells and in OP9 cell lines (Figures 5C-F, S4D-E). The upregulated *miR-155* was functional, as shown by the target luciferase assay (Figure S4F). As RBPJ is a transcriptional repressor, we hypothesized that RBPJ associates with the *miR-155* promoter and suppresses its transcription. *In silico* analysis of the *BIC/miR-155* promoter revealed the presence of two putative RBPJ binding sites (Jarriault et al., 1995) at -1792 and at -1703 nt upstream of the start site (Figure 5G). Chromatin immunoprecipitation analysis (ChIP) of the promoter using primers (Table S1) for these two regions confirmed binding of endogenous RBPJ to the endogenous *miR-155* promoter in cells derived from *RBPJ*$^{+/+}$ mice but not *RBPJ*$^{-/-}$ mice (Figure 5H, left panel). Similarly, binding of RBPJ to *miR-155* promoter was observed in EC and Raw cells and was abrogated following the expression of *shRBPJ* (Figure 5H, middle and right panels). Notch was also found in the complex when RBPJ was present (Figure S4G). To further confirm the repressor activity of RBPJ on the *miR-155* promoter, we cloned the 2kb *pre-miR-155* promoter region containing the two RBPJ binding sites into a luciferase reporter construct. Consistent with a repressor function of RBPJ, *miR-155* transcriptional activation was increased 2 to 3 fold following *RBPJ* repression (Figure 5I). *miR-155* expression was also increased following treatment of Raw cells with the γ-secretase inhibitor (GSI; Figure 5I), which inhibits the generation of NICD and ultimately prevents the formation of the NICD/RBPJ complex on the promoter. Conversely, overexpression of NICD decreased *miR-155* expression in Raw cells and in T-cells (Figure S4H-I). As RBPJ has been shown to associate with the histone deacetylase complex (HDAC) (Kao et al., 1998), and HDAC2 binding is observed at the *miR-155* promoter in wild-type Raw cells (Figure S4J), we investigated whether RBPJ regulated *miR-155* repression through HDAC function. Treatment with a pan HDAC inhibitor led to a 3 fold increase in the expression of *miR-155*, similar to the effect induced by deletion of RBPJ (Figure 5I).

miR-155 induces *G-CSF* and *TNFα* expression via NF-κB activation

Given the strong correlation between *miR-155* upregulation and increased G-CSF and TNFα levels, we hypothesized that *miR-155* regulates G-CSF and TNFα production by BM stromal cells. Transfection of *shRBPJ* in ECs and Raw cells resulted in increased *G-CSF* and *TNFα* expression and protein levels (Figure 6A-B and S5A) and enhanced their ability to promote myeloid cell expansion in co-culture (Figure 6C). Similarly, overexpression of *miR-155* in Raw cells resulted in rapid up-regulation of G-CSF and TNFα (Figure 6D). Consistently, treatment of *RBPJ* knocked down cells with an anti-*miR-155* LNA inhibited *shRBPJ*-mediated induction of *G-CSF* and *TNFα* (Figure 6E and S5B). Thus, loss of *RBPJ* augments G-CSF and TNFα levels by directly up-regulating the expression of *miR-155*. To identify the molecular link between *miR-155* and inflammatory cytokines, we used the microRNA target predictions program https://cm.jefferson.edu/rna22v1.0-musmusculus/ (Miranda et al., 2006) and searched for putative *miR-155* targets whose inhibition might result in the transcriptional activation of *G-CSF* and *TNFα*. Among the predicted targets, the NF-κB inhibitor κB-Ras1 (also known as Nkiras1) that inhibits IkB-β phosphorylation

(Fenwick C, Science 2000), was found to have *miR-155* target sequences at its 3′UTR. Given that the inflammatory profile observed in *RBPJ*^{-/-} stromal cells has a NF-κB signature (Figure S2) and that the transcription of *G-CSF* and *TNFα* is regulated principally by NF-κB, we tested the hypothesis that *miR-155* up-regulation increased NF-κB activation by decreasing its inhibition. κB-Ras1 protein levels were noticeably reduced in *RPBJ*^{-/-} mice (Figure S5C) and *κB-Ras1* expression was significantly decreased in *RPBJ*^{-/-} BM stroma (Figure 6F). In Raw cells, *κB-Ras1* expression was significantly reduced by repressing *RBPJ or* by overexpressing *miR-155* (Figure 6G). Importantly, *κB-Ras1* downregulation in these cells was antagonized by *miR-155* LNA (Figure 6H). Next, we cloned the κB-Ras1 3′UTR into the pMIR-RL vector and confirmed that κB-Ras1 is a bona fide *miR-155* target, as shown by decreased luciferase activity in response to *miR-155* overexpression (Figure 6I). Targeting of κB-Ras1 by shRNA (shκB-Ras1) increased expression of *G-CSF* and *TNFα* in both Raw and EC cells (Figure 6J-K). *κB-Ras1* inhibition correlated with increased transcriptional activation of *NF-κB* in Raw shRBPJ and Raw MSCV-miR155 expressing cells (Figure 6L) and inhibition of NF-κB by the NF-κB inhibitor DMAPT (dimethylamino-parthenolide) (Neelakantan et al., 2009), resulted in a significant decrease in the expression of *G-CSF* and *TNFα* (Figure 6M). Finally, analysis of *miR-155, κB-Ras1, G-CSF* and *TNFα* expression, showed that sorted BM EC and MSC from *RBPJ*^{-/-}mice had the highest expression of *miR-155*, correlating with the lowest expression of *κB-Ras1* and higher levels of *G-CSF* and *TNFα*, compared to purified osteoblasts and sorted CD45^{+} cells (Figure S5D).

Taken together, our results demonstrate that, following Notch/RBPJ loss of function, miR-155 up-regulates NF-κB activation by targeting one of its inhibitors, κB-Ras1, leading to increased expression of G-CSF and TNFα. Furthermore, these results suggest that this axis may be cell context-dependent and likely to be more active in BM EC and MSC.

miR-155 is required for the development of RBPJ-dependent myeloproliferative-like disease and is upregulated in the BM of MPN patients

To examine the impact of *miR-155* deletion on *RBPJ* dependent MPN development, we generated *Mx1RBPJ*[lox/lox]*/miR-155*^{-/-} (*DKO*) and *Mx1RBPJ*[lox/lox]*/miR-155*^{+/+} (*KO*) littermates. Consistent with our previous results, deletion of RBPJ induced a lethal myeloproliferative-like disease and *KO* mice died within 20 weeks of pIpC treatment. In contrast, all *DKO* mice remained viable at this same time point. Comparative analysis of the hematopoietic compartment in these mice showed that neutrophils increased dramatically in the PB of *KO* mice, while *DKO* mice exhibited normal levels of PB neutrophils (Figure 7A), lacked the development of splenomegaly (Figure S6A) and showed only a modest increase in CMP and GMPs in the BM compared to *KO* mice (Figure 7B). Importantly, G-CSF levels in the serum of DKO recipients were similar to those seen in healthy controls (Figure S6B).

To prove that *miR-155* knock down in the stroma is critical for myeloid cell expansion, we transplanted WT BM cells into lethally irradiated DKO and KO mice. As anticipated, KO recipients developed disease, whereas deletion of *miR-155* in the stroma of DKO recipients correlated with only a modest increase in Gr1^{+}/Mac1^{+} cells in the PB (Figure 7C), prevented the development of splenomegaly and the increase of myeloid progenitors (CMP and GMP) in the BM (Figure 7D-E). Histologic analysis of the DKO recipients showed absence of the

myeloid expansion with normal myeloid/erythroid ratio in the BM and intact structure of the spleen (Figure 7G). A significant decrease of *κB-Ras1* expression was observed in sorted KO BM EC and MSC compared to WT cells (Figure S5D). Conversely, the levels of *κB-Ras1* were increased or restored to normal in sorted DKO BM EC and MSC compared to KO cells (Figure 7F). The normalization of *κB-Ras1* expression in DKO cells correlated with the normalization of *G-CSF* and *TNFα* expression.

Taken together, these experiments show a key role for *miR-155* in sustaining the inflammatory reaction driving the lethal myeloproliferative-like disease triggered by the loss of RBPJ. To determine the potential clinical relevance of our observations, we examined whether *miR-155* was also altered in patients with myeloproliferative neoplasia (MPN) characterized by a high inflammatory component, such as myelofibrosis (MF). Analysis of 85 MF patients revealed a significant increase in the expression of *miR-155* in total BM cells compared to normal control patients (Figure 7H), whereas an increase was not detected in mononuclear cells of the PB (data not shown). Collectively, this observation suggests that *miR-155* may play a role in the human disease and may represent a potential therapeutic target for the control of myeloid cell expansion.

Discussion

Evidence supporting a non-cell-autonomous role for Notch signaling in the regulation of hematopoiesis has recently emerged; however, the cellular and molecular mechanism(s) by which Notch regulates the integrity of the BM niche are still poorly understood. By using a Notch/RBPJ loss-of-function model we demonstrated that RBPJ functions as a transcriptional repressor of the microRNA *miR-155:* a microRNA involved in inflammation and frequently up-regulated in leukemia cells and solid tumors. *miR155* up-regulation due to loss of the Notch/RBPJ axis increased NF-κB activation by targeted inhibition of κB-Ras1 and induced a persistent pro-inflammatory state of the BM niche leading to a myeloproliferative-like disease.

Global (canonical and non-canonical) loss of Notch signaling, due to deletion of Mindbomb (Kim et al., 2008b), ADAM10 (Yoda et al., 2011) or Pofut1 (Yao et al., 2011) has been correlated with the development of a myeloproliferative-like syndrome driven by both cell-autonomous and non-cell autonomous mechanisms, whereas deletion of Nicastrin has been shown to lead instead to a cell-autonomous chronic myelo-monocytic leukemia (CMML)-like disease (Klinakis et al., 2011). Discrepancies among these models may be due to the contribution of other targets regulated by ADAM10 (Pruessmeyer and Ludwig, 2009), Pofut1 and the Nicastrin γ-secretase complex (De Strooper, 2005), which acting in combination with global Notch loss-of-function may account for the variable involvement of the microenvironment. However, the molecular mechanisms linking loss of Notch signaling with altered myelopoiesis were not defined in these models.

Our study clearly shows that loss of RBPJ, a non-redundant downstream effector of canonical Notch signaling, is necessary and sufficient to induce a lethal myeloproliferative-like disease driven by the microenvironment. *RBPJ*$^{-/-}$ stem and progenitor cells were not capable of inducing myeloid expansion or a myeloproliferative disease in a cell-autonomous

manner. This effect was further confirmed by using the *Lys-CreRBPJ^lox/lox* model, in which the RBPJ deletion occurs only in the myeloid progenitors starting at the CMP stage (Figure S3F-G). Of note, our studies clearly uncouple the direct, cell autonomous role of Notch/ RBPJ signaling on HSC homeostasis from its non-cell autonomous impact on myeloid progenitors. Interestingly, lymphocytosis was observed only in the parental *RBPJ^-/-* mice but not in the BM chimeras, suggesting that this process requires both cell autonomous and non-cell autonomous mechanisms; further studies are warranted to understand the impact of RBPJ loss on this process.

Here, we unveil a previously unrecognized link between RBPJ-dependent Notch signaling and *miR-155*. RBPJ represses transcription by binding to specific sequence motifs in the promoter of target genes and by recruiting co-repressors such SMRT and SHARP (Oswald et al., 2005) and the HDAC complex (Kao et al., 1998). Our study shows that RBPJ binds to the *miR-155* promoter and that either deletion of *RBPJ* DNA binding domain or loss of full-length RBPJ causes *miR-155* up-regulation. Importantly, our data show that RBPJ-mediated repression of *miR-155* is NICD-dependent, suggesting the possibility that Notch may also function as a transcriptional repressor. This is intriguing considering that it is well established that NICD converts RBPJ from a transcriptional repressor to a transcriptional activator (Kopan and Ilagan, 2009). However, precedents of Notch signaling as repressor have been reported and involved dislocation and recruitment of coactivators and corepressors, respectively (Sakano et al., 2010; Tiberi et al., 2012). Alternatively, it is posible that the association of NICD to RBPJ, which can enhance its binding to a specific promoter (Krejci and Bray, 2007; Castel et al., 2013), may result in RBPJ repressor function on the *miR-155* promoter; however, whether the presence of NICD on the *miR-155* promoter enhances RBPJ repressor activity directly or indirectly needs to be further investigated. Collectively, these data support the possibility that *miR-155* expression may be physiologically regulated by tuning of the Notch signaling and may indicated a more general mechanism of *miR-155* regulation through repression. This hypothesis is supported by a recent study reporting inhibition of *miR-155* by transcriptional repression in breast cancer cells, where mutation in the tumor suppressor BRCA1 gene abolishes its repressive function on the *miR-155* promoter, resulting in increased *miR-155* expression in breast cancer cells and in tumor progression (Chang et al., 2011).

miR-155 plays a broad role in inflammation and in the regulation of the immune-system and it is induced by a wide range of inflammatory factors including LPS/TLR responses. Although increased expression of *miR-155* has been positively associated with increased cytokine production, in particular G-CSF and TNFα (Tili et al., 2009; Worm et al., 2009) the molecular mechanism(s) by which *miR-155* enhances the expression of these cytokines were not investigated. Our results show that *miR-155* increases NF-κB activation by targeting one of its negative regulators, κB-Ras1 (Fenwick et al., 2000). κB-Ras1 (also known as Nkiras1) is a small protein with similarity to Ras-like small GTPases that functions as a negative modulator of NF-κB by binding to NF-κB/IκB complexes and preventing lκBβ and IκBα phosphorylation by IKK (Chen et al., 2004). κB-Ras1 is ubiquitously expressed and its levels inversely correlate with poor prognosis in tumors. While prior studies have suggested an important role for NF-κB in regulating *miR-155*

expression (Baltimore et al., 2008), our findings reveal that *miR-155* can reciprocally upregulate NF-κB activity and amply the inflammatory response by inducing NF-κB-dependent cytokines, in particular G-CSF and TNFα.

A previous report demonstrated a cell intrinsic role for *miR-155* in driving myeloproliferative-like disease in a murine transduction/transplantation model (O'Connell et al., 2008). Our findings clearly demonstrate a non-cell autonomous mechanism by which *miR-155* overexpression contributes to a myeloproliferative-like disease in RBPJ deficient mice. Interestingly, while *RBPJ*$^{-/-}$ progenitors exhibit *miR-155* up-regulation, transplantation of these cells in WT recipients did not lead to a myeloid expansion. This discrepancy is likely due to the differential expression of *miR-155* in the two murine models as well as to differences in the cell types producing this micro-RNA. As discussed by Tili and Croce (Tili et al., 2009), the differential impact of *miR-155* on its targets can depend significantly on the level of its expression. Thus, in contrast to models of forced expression, resulting in a ∼30 fold increase of *miR-155* on hematopoietic cells compared to normal levels (O'Connell et al., 2008), the *miR-155* levels reached in our model (3-5 fold increase) were likely not enough to drive a cell-autonomous MPN, but were sufficient to drive cytokine production in cells of the BM microenvironment specialized to generate an inflammatory response, such as endothelial cells. Our studies point to cell context differences and a higher ability of BM EC and MSC to activate the miR-155/NF-κB/G-CSF/TNFα pathway compared to hematopoietic cells and osteoblasts. Indeed, we show that RBPJ deletion in endothelial cells is sufficient to drive a myeloproliferative-like disease. A relevant role of ECs in this process is not surprising, given that stem cells and progenitors localize adjacent to sinusoids in the BM and that ECs are poised to regulate the hematopoietic response during inflammation through production of pro-inflammatory cytokines (Ding et al., 2012; Fernandez et al., 2008)

Both G-CSF and TNFα are commonly upregulated upon TLR-mediated stimulation during emergency granulopoiesis and following infections (Hirai et al., 2006; Ueda et al., 2005). Their increased expression is also a common feature of several animal models of myeloproliferative-like disease (Dumortier et al., 2010; Fulzele et al., 2013; Walkley et al., 2007; Yoda et al., 2011) and it is observed in patients with MPN (Tefferi et al., 2011). Our discovery of the Notch/miR155/NF-κB/cytokines axis suggests the hypothesis that Notch signaling may contribute to hematopoietic homeostasis by regulating the level of the inflammatory state in the BM niche. In support of this idea, a recent report noted physiologic downregulation of Notch signaling in response to LPS (Kim et al., 2008a); furthermore epigenetic silencing of Notch in myeloid malignancies has been documented (Lobry et al., 2013). Thus, while transitory inhibition of Notch signaling in the BM microenvironment may trigger a physiologic inflammatory circuit characterized by miR-155/NF-κB/cytokine induction driving myeloid cell expansion in response to BM stress (such as infection or acute inflammation), continuous inhibition of Notch signaling due to persistence of inflammatory feed-back loops or/and epigenetic mechanisms, may contribute to the development or progression of a myeloproliferative disorder.

Consistent with our observations demonstrating an essential role for Notch/RBPJ in regulating *miR-155* and driving a myeloproliferative-like disease in a murine model, we

observed a significant overexpression of *miR-155* in Myelofibrosis (MF) patients' BM samples (enriched in stromal cellular components), but not in the PB. Relevant to these findings is the notion that NF-κB plays an essential role in multiple myeloid malignancies and that a comprehensive cytokine profile on serum derived from MF patients demonstrated a cytokine profile very similar to that observed in our mouse model of RBPJ deficiency (Tefferi et al., 2011). Collectively these findings provide a strong link between miR-155/NF-κB and MPN and the rationale to explore this molecular axis to target inflammation and disease progression in these diseases.

Experimental Procedures

Mice

RBPJ^{lox/lox} mice were obtained from T. Honjo; *Tie2Cre^{ER}* mice were obtained from B. Arnold (European Mouse Mutant Archive; Monterotondo, Italy); *miR-155^{-/-}* and Lys-Cre mice were obtained from Jackson Laboratories; Lys-EGFP mice were obtained from Dr. T. Graf; DMP1Cre/RBPJ^{-/-} mice were obtained from Dr. T.Bellido. Mx1-Cre recombinase was induced by pIpC 200μg i.p., 3 times at 2-day interval (wk1) plus one single dose (wk2). Efficiency of RBPJ excision was assessed by qRT-PCR (primers in Table S1); *Tie2Cre^{ER}* expression was induced by tamoxifen 100mg/kg body for 4-5 weeks, twice/day by gavage. Animal experiments were performed using protocols approved by the IUSM Animal Care and Use Committee.

Cells and cell culture

Raw264.7 and OP9 cells were cultured in DMEM and α-MEM with 10%FBS at 37°C. Cells were transfected with pLKO.1-shRBPJ construct (Thermo) or pLKO.1 vector; or with psiLvU6-shκB-Ras1 or control vector (Genecopoeia) using Lipofectamine 2000 reagent (Life Technologies); or with the retroviral vectors MSCV-GFP, MSCV-ICN/GFP or MGP M155 (MSCV-miR-155, Addgene). BM stromal cells were generated from long bones (tibias, femurs) pre-incubated with 1% collagenase. Total BM cells were flushed and cultured in α-MEM with 20% FBS. Non-adherent cells were removed after 2 days of culture, and adherent cells were expanded for 1wk prior sorting to purify CD45⁻ BM stromal cells by CD45 microbeads (Miltenyi Biotec).

Mouse lung microvascular endothelial cells (Kuhlencordt et al., 2004) were provided by I. Petrache. Cells were grown in DMEM with 20% FBS. Osteoblasts were obtained by long bones as described (Chitteti et al, 2010).

Co-cultures: Lin⁻ cells were purified from femur's BM using the lineage-cell depletion kit (Miltenyi), plated at a density of 5×10^4/ml on a confluent BM stromal cell layer, and cultured for 48 hrs in IMDM (Gibco, Invitrogen) containing 10% FBS, 50ng/mL SCF and 50ng/mL IL-3 (Miltenyi). Raw cells were treated with 1 μM GSI (EMD Calbiochem), 1 μM HDAC inhibitor (Vorinostat) or 5μM DMAPT for 24 or 48 hours. LNA treatment: cells were transfected with 75nM LNA scramble or anti-miR-155 (Exiqon Company) using lipofectamine 2000 (Invitrogen). Cells were collected for analysis at d2 and d4 post-transfection.

Patients Cells

Primary patients' BM aspirates were obtained from MPN patients with MF seen at the University of Texas MD Anderson Cancer Center, and normal BM cells samples were obtained from Stem Cell Technologies (Vancouver, Canada). BM cells were fractionated using Ficoll Hypaque 1077 (Sigma-Aldrich).

Flow cytometry and cell sorting

BM, spleen and PB cell suspensions were labeled with monoclonal antibodies (Abs) used to define distinct hematopoietic subsets (Table S2). Cells were acquired on a LSRII (BD) and events (0.5 to 5×10^6/staining) collected and analyzed using Flowjo. CD45^{-}CD31^{+}CD105^{+} and CD45^{-}CD31^{-}CD105^{+} cells were sorted in the Reflection3 cell sorter from total BM cells after staining with CD45-APC, CD31-FITC and CD105-PE .

Bone Marrow Transplantation

Total BM cells (5×10^6) from pIpC-induced *Mx-Cre[+] RBPJ[lox/lox]* or control *Mx-Cre[−]* littermates (CD45.2) were transplanted by tail vein injection into lethally irradiated B6-SJL (CD45.1) recipients. Total BM cells (3×10^6) from CD45.1 WT or Lys-EGFP mice were transplanted into irradiated, pIpC-induced *Mx-Cre+ RBPJ[lox/lox] or* control *Mx-Cre[−]* recipient mice.

Histology: Tissues were fixed in Z-fix buffer, paraffin-embedded, sectioned, and stained with hematoxylin-eosin.

G-CSF Ab in vivo

Mx1Cre[+] and *Mx1Cre[-] RBPJ[lox/lox]* 6 to 8wk-old mice were induced with pIpC and after 6 wks were treated with anti-G-CSF neutralizing Ab (R&D # AB-414-NA) 10 μg/d i.p. for 2 cycles of 12 days.

Cytokine array and ELISA

BM milieu was obtained by flashing 1 femur with 1ml of Milliplex reagent; serum was collected from PB; BM-stroma supernatants at 72hrs collection were used. Cytokine levels were measured using a mouse cytokine array (R&D) and Luminex MAP assays (MILLIPLEX MAP Mouse Cytokine/Chemokine, Millipore # MCYTOMAG-70K-09).

Quantitative RT-PCR and microRNA quantification

RNA was purified with the RNeasy Mini Kit (QIAGEN) and cDNA prepared using the Superscript II Kit (Invitrogen). qRT-PCR was performed using SYBR green II Brilliant (Stratagene); Primers are shown in Table S1.

Total RNA from BM sorted cells, BM-derived stroma and Raw cells were extracted with RNAqueous Micro Kit (Ambion). MicroRNA expression was assessed by qRT-PCR (Applied Biosystems) using microRNA-specific TaqMan MicroRNA Assays (mmu-miR-155, U6snRNA). BM from healthy donors and PMF patients was extracted using Trizol (Invitrogen) and 10ng of total RNA from each sample was transcribed using the Taqman

MicroRNA reverse Transcriptase kit on ABI 7900HT FAST platform (Applied Biosystems). miR-155 and control gene RUN6B (Applied Biosystems) expression were analyzed by qRT-PCR, using Taqman probes.

Cloning of miR-155 and promoter, κB-Ras1 3′UTR, gene reporter assay and ChIP analysis

The mouse miR-155 promoter region (-1842 to -18) containing the RBPJ binding sites was amplified by PCR from C57BL/6 mouse spleen genomic DNA (primers in table S1). Cloning was performed into the site between XhoI and HindIII of the pGL4.10 luciferase reporter vector (Promega) and confirmed by sequencing. A Dual-Luciferase Assay (Promega) was performed to quantify miR-155 promoter activity. Raw cells were co-transfected with pGL4.10/miR-155Luc and the CMV/Renilla luc control plasmid. The mouse κB-Ras1 3′UTR region (+779 to +4592) containing two miR155 binding sites was amplified by PCR from C57BL/6 mouse genomic DNA (primers in table S1). Cloning was performed into the site between SacI and PmeI of the pmiR-RL vector. Raw cells were co-transfected with the pmiR-RL vector and the CMV/Renilla luc control plasmid to determine targeting of the κB-Ras1 3′UTR by miR155. miR-155 levels and function were also measured in cells by co-transfecting a firefly luciferase reporter containing a binding site for miR-155 at 3′UTR downstream of the luciferase gene (Signosis) and the control Renilla plasmid. Luminescence was measured 24-48hrs after transfection, using a TD-20/20 luminometer (Turner Biosystems).

Chromatin preparations from $RBPJ^{-/-}$ and $RBPJ^{+/+}$ BM cells, or Raw transfected with shRBPJ or scrambled shRNA, were cross-linked with endogenous DNA and immunoprecipitated with anti-RBPJ (Santa Cruz, 28713)(Barbarulo et al., 2011), anti-Notch1 (Santa Cruz, 6014-R), anti-HDAC2(Cell Signaling, 2545S). As negative controls IgG or irrelevant antibodies (anti-Jagged1; Santa Cruz, 8303) were used; anti-PolII was used as positive control. Recovered DNA was analyzed for miR-155 and GAPDH (control) promoter fragments by qRT-PCR using specific primers (TableS1).

Imaging acquisition and image analysis

Two-photon images of calvarium BM were collected using Olympus XLUMPLFL 20xW, NA 0.95 objective. Z-stacks were collected through the depth of tissue (60 μm Z-stacks) from 6 regions of calvarium BM, at step size settings of 1 μm and 512x512 pixels frame size. Projection images were created using MetaMorph imaging software (Molecular 135 Devices). Volume rendering software Voxx was used to create 3D reconstructions of BM.

Statistical Analysis

Equality of distributions for matched pairs of observations was tested using the *t* test. Survival was calculated using Kaplan-Meier calculations. *P*<0.05 was considered to be statistically significant.

Supplementary Material

Refer to Web version on PubMed Central for supplementary material.

Acknowledgments

References

Artavanis-Tsakonas S, Rand MD, Lake RJ. Notch signaling: cell fate control and signal integration in development. Science. 1999; 284:770–776. [PubMed: 10221902]

Baltimore D, Boldin MP, O'Connell RM, Rao DS, Taganov KD. MicroRNAs: new regulators of immune cell development and function. Nat Immunol. 2008; 9:839–845. [PubMed: 18645592]

Barbarulo A, Grazioli P, Campese AF, Bellavia D, Di Mario G, Pelullo M, Ciuffetta A, Colantoni S, Vacca A, Frati L, et al. Notch3 and canonical NF-kappaB signaling pathways cooperatively regulate Foxp3 transcription. J Immunol. 2011; 186:6199–6206. [PubMed: 21508258]

Castel D, Mourikis P, Bartels SJ, Brinkman AB, Tajbakhsh S, Stunnenberg HG. Dynamic binding of RBPJ is determined by Notch signaling status. Genes Dev. 2013; 27:1059–1071. [PubMed: 23651858]

Chang S, Wang RH, Akagi K, Kim KA, Martin BK, Cavallone L, Haines DC, Basik M, Mai P, Poggi E, et al. Kathleen Cunningham Foundation Consortium for Research into Familial Breast Cancer (kConFab). Tumor suppressor BRCA1 epigenetically controls oncogenic microRNA-155. Nat Med. 2011; 17:1275–1282. [PubMed: 21946536]

Chen Y, Vallee S, Wu J, Vu D, Sondek J, Ghosh G. Inhibition of NF-kappaB activity by IkappaBbeta in association wtih kappaB-Ras. Mol cell Biol. 2004; 24:3048–3056. [PubMed: 15024091]

Chitteti BR, Cheng YH, Streicher DA, Rodriguez-Rodriguez S, Carlesso N, Srour EF, Kacena MA. Osteoblast lineage cells expressing high levels of Runx2 enhance hematopoietic progenitor cell proliferation and function. J Cell Biochem. 2010; 111:284–294. [PubMed: 20506198]

Davis RL, Turner DL. Vertebrate hairy and Enhancer of split related proteins: transcriptional repressors regulating cellular differentiation and embryonic patterning. Oncogene. 2001; 20:8342–8357. [PubMed: 11840327]

De Strooper B. Nicastrin: gatekeeper of the gamma-secretase complex. Cell. 2005; 122:318–320. [PubMed: 16096051]

De Strooper B, Annaert W, Cupers P, Saftig P, Craessaerts K, Mumm JS, Schroeter EH, Schrijvers V, Wolfe MS, Ray WJ, et al. A presenilin-1-dependent gamma-secretase-like protease mediates release of Notch intracellular domain. Nature. 1999; 398:518–522. [PubMed: 10206645]

Ding L, Saunders TL, Enikolopov G, Morrison SJ. Endothelial and perivascular cells maintain haematopoietic stem cells. Nature. 2012; 481:457–462. [PubMed: 22281595]

Dumortier A, Durham AD, Di Piazza M, Vauclair S, Koch U, Ferrand G, Ferrero I, Demehri S, Song LL, Farr AG, et al. Atopic dermatitis-like disease and associated lethal myeloproliferative disorder arise from loss of Notch signaling in the murine skin. PloS one. 2010; 5:e9258. [PubMed: 20174635]

Faust N, Varas F, Kelly LM, Heck S, Graf T. Insertion of enhanced green fluorescent protein into the lysozyme gene creates mice with green fluorescent granulocytes and macrophages. Blood. 2000; 96:719–726. [PubMed: 10887140]

Fenwick C, Na SY, Voll RE, Zhong H, Im SY, Lee JW, Ghosh S. A subclass of Ras proteins that regulate the degradation of IkappaB. Science. 2000; 287:869–873. [PubMed: 10657303]

Fernandez L, Rodriguez S, Huang H, Chora A, Fernandes J, Mumaw C, Cruz E, Pollok K, Cristina F, Price JE, et al. Tumor necrosis factor-alpha and endothelial cells modulate Notch signaling in the bone marrow microenvironment during inflammation. Exp Hematol. 2008; 36:545–558. [PubMed: 18439488]

Forde A, Constien R, Grone HJ, Hammerling G, Arnold B. Temporal Cre-mediated recombination exclusively in endothelial cells using Tie2 regulatory elements. Genesis. 2002; 33:191–197. [PubMed: 12203917]

Fulzele K, Krause DS, Panaroni C, Saini V, Barry KJ, Liu X, Lotinun S, Baron R, Bonewald L, Feng JQ, et al. Myelopoiesis is regulated by osteocytes through Gsalpha-dependent signaling. Blood. 2013; 121:930–939. [PubMed: 23160461]

Han H, Tanigaki K, Yamamoto N, Kuroda K, Yoshimoto M, Nakahata T, Ikuta K, Honjo T. Inducible gene knockout of transcription factor recombination signal binding protein-J reveals its essential role in T versus B lineage decision. International immunology. 2002; 14:637–645. [PubMed: 12039915]

Hirai H, Zhang P, Dayaram T, Hetherington CJ, Mizuno S, Imanishi J, Akashi K, Tenen DG. C/EBPbeta is required for 'emergency' granulopoiesis. Nat Immunol. 2006; 7:732–739. [PubMed: 16751774]

Jarriault S, Brou C, Logeat F, Schroeter EH, Kopan R, Israel A. Signalling downstream of activated mammalian Notch. Nature. 1995; 377:355–358. [PubMed: 7566092]

Kao HY, Ordentlich P, Koyano-Nakagawa N, Tang Z, Downes M, Kintner CR, Evans RM, Kadesch T. A histone deacetylase corepressor complex regulates the Notch signal transduction pathway. Genes Dev. 1998; 12:2269–2277. [PubMed: 9694793]

Kim MY, Park JH, Mo JS, Ann EJ, Han SO, Baek SH, Kim KJ, Im SY, Park JW, Choi EJ, et al. Downregulation by lipopolysaccharide of Notch signaling, via nitric oxide. Journal of cell science. 2008a; 121:1466–1476. [PubMed: 18411251]

Kim YW, Koo BK, Jeong HW, Yoon MJ, Song R, Shin J, Jeong DC, Kim SH, Kong YY. Defective Notch activation in microenvironment leads to myeloproliferative disease. Blood. 2008b; 112:4628–4638. [PubMed: 18818392]

Klinakis A, Lobry C, Abdel-Wahab O, Oh P, Haeno H, Buonamici S, van De Walle I, Cathelin S, Trimarchi T, Araldi E, et al. A novel tumour-suppressor function for the Notch pathway in myeloid leukaemia. Nature. 2011; 473:230–233. [PubMed: 21562564]

Kopan R, Ilagan MX. The canonical Notch signaling pathway: unfolding the activation mechanism. Cell. 2009; 137:216–233. [PubMed: 19379690]

Krejci A, Bray S. Notch activation stimulates transnient and selective binding of Su(H)/CSL to target enhancers. Genes Dev. 2007; 21:1322–1327. [PubMed: 17545467]

Kuhlencordt PJ, Rosel E, Gerszten RE, Morales-Ruiz M, Dombkowski D, Atkinson WJ, Han F, Preffer F, Rosenzweig A, Sessa WC, et al. Role of endothelial nitric oxide synthase in endothelial activation: insights from eNOS knockout endothelial cells. American journal of physiology Cell physiology. 2004; 286:C1195–1202. [PubMed: 15075219]

Lobry C, Ntziachristos P, Ndiaye-Lobry D, Oh P, Cimmino L, Zhu N, Araldi E, Hu W, Freund J, Abdel-Wahab O, et al. Notch pathway activation targets AML-initiating cell homeostasis and differentiation. J Exp Med. 2013; 210:301–319. [PubMed: 23359070]

Miranda KC, Huynh T, Tay Y, Ang YS, Tam WL, Thomson AM, Lim B, Rigoutsos I. A pattern-based method for the identification of MicroRNA binding sites and their corresponding heteroduplexes. Cell. 2006; 126:1203–1217. [PubMed: 16990141]

Miyamoto T, Iwasaki H, Reizis B, Ye M, Graf T, Weissman IL, Akashi K. Myeloid or lymphoid promiscuity as a critical step in hematopoietic lineage commitment. Developmental cell. 2002; 3:137–147. [PubMed: 12110174]

Neelakantan S, Nasim S, Guzman ML, Jordan CT, Crooks PA. Aminoparthenolides as novel anti-leukemic agents: Discovery of the NF-kappaB inhibitor, DMAPT (LC-1). Bioorganic & medicinal chemistry letters. 2009; 19:4346–4349. [PubMed: 19505822]

O'Connell RM, Rao DS, Chaudhuri AA, Boldin MP, Taganov KD, Nicoll J, Paquette RL, Baltimore D. Sustained expression of microRNA-155 in hematopoietic stem cells causes a myeloproliferative disorder. J Exp Med. 2008; 205:585–594. [PubMed: 18299402]

Oswald F, Winkler M, Cao Y, Astrahantseff K, Bourteele S, Knochel W, Borggrefe T. RBP-Jkappa/SHARP recruits CtIP/CtBP corepressors to silence Notch target genes. Mol Cell Biol. 2005; 25:10379–10390. [PubMed: 16287852]

Pruessmeyer J, Ludwig A. The good, the bad and the ugly substrates for ADAM10 and ADAM17 in brain pathology, inflammation and cancer. Seminars in cell & developmental biology. 2009; 20:164–174. [PubMed: 18951988]

Sakano D, Kato A, Parikh N, McKnight K, Terry D, Stefanovic B, Kato Y. BCL6 canalizes Notch-dependent transcription, excluding Mastermind-like1 from selected target genes during left-right patterning. Developmental cell. 2010; 18:450–462. [PubMed: 20230751]

Schneider A, Zhang Y, Guan Y, Davis LS, Breyer MD. Differential, inducible gene targeting in renal epithelia, vascular endothelium, and viscera of Mx1Cre mice. Am J Physiol Renal Physiol. 2003; 284:F411–F417. [PubMed: 12529277]

Tefferi A, Vaidya R, Caramazza D, Finke C, Lasho T, Pardanani A. Circulating interleukin (IL)-8, IL-2R, IL-12, and IL-15 levels are independently prognostic in primary myelofibrosis: a comprehensive cytokine profiling study. J Clin Oncol. 2011; 29:1356–1363. [PubMed: 21300928]

Tiberi L, van den Ameele J, Dimidschstein J, Piccirilli J, Gall D, Herpoel A, Bilheu A, Bonnefont J, Iacovino M, Kyba M, et al. BCL6 controls neurogenesis through Sirt1-dependent epigenetic repression of selective Notch targets. Nature neuroscience. 2012; 15:1627–1635.

Tili E, Croce CM, Michaille JJ. miR-155: on the crosstalk between inflammation and cancer. Int Rev Immunol. 2009; 28:264–284. [PubMed: 19811312]

Tili E, Michaille JJ, Croce CM. MicroRNAs play a central role in molecular dysfunctions linking inflammation with cancer. Immunol Rev. 2013; 253:167–184. [PubMed: 23550646]

Ueda Y, Kondo M, Kelsoe G. Inflammation and the reciprocal production of granulocytes and lymphocytes in bone marrow. J Exp Med. 2005; 201:1771–1780. [PubMed: 15939792]

Walkley CR, Olsen GH, Dworkin S, Fabb SA, Swann J, McArthur GA, Westmoreland SV, Chambon P, Scadden DT, Purton LE. A microenvironment-induced myeloproliferative syndrome caused by retinoic acid receptor gamma deficiency. Cell. 2007; 129:1097–1110. [PubMed: 17574023]

Worm J, Stenvang J, Petri A, Frederiksen KS, Obad S, Elmen J, Hedtjarn M, Straarup EM, Hansen JB, Kauppinen S. Silencing of microRNA-155 in mice during acute inflammatory response leads to derepression of c/ebp Beta and down-regulation of G-CSF. Nucleic Acids Res. 2009; 37:5784–5792. [PubMed: 19596814]

Yao D, Huang Y, Huang X, Wang W, Yan Q, Wei L, Xin W, Gerson S, Stanley P, Lowe JB, et al. Protein O-fucosyltransferase 1 (Pofut1) regulates lymphoid and myeloid homeostasis through modulation of Notch receptor ligand interactions. Blood. 2011; 117:5652–5662. [PubMed: 21464368]

Yoda M, Kimura T, Tohmonda T, Uchikawa S, Koba T, Takito J, Morioka H, Matsumoto M, Link DC, Chiba K, et al. Dual functions of cell-autonomous and non-cell-autonomous ADAM10 activity in granulopoiesis. Blood. 2011; 118:6939–6942. [PubMed: 22042698]
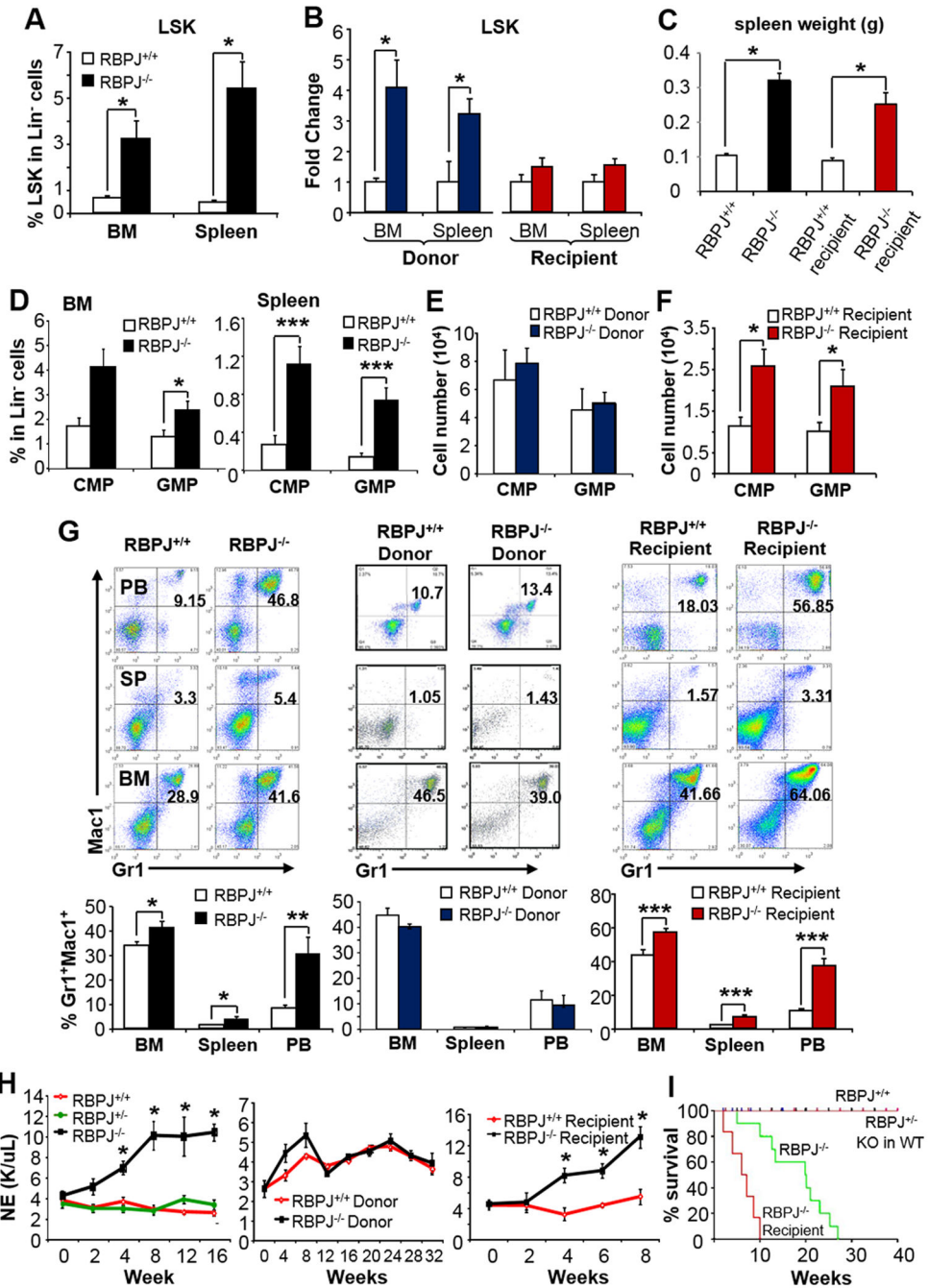
Highlights

- Notch/RBPJ functions as a transcriptional repressor of miR-155

- miR-155 targets the NF-kB inhibitor kB-Ras1 increasing NF-kB activation

- Loss of endothelial Notch/RBPJ signaling increases NF-kB activation via miR155

- Persistent miR155/NF-kB activation in the BM niche drives myeloproliferation

Figure 1. Cell-autonomous and non-cell autonomous impact of *RBPJ* deletion in the hematopoietic compartment

(A) % of LSK cells in BM and spleen of *RBPJ*^{-/-} and *RBPJ*^{+/+} mice at 15-20 wks after pIpC (n=8-12).

(B) LSK cells in BM and spleen of WT (CD45.1) recipient mice transplanted with CD45.2[+] *RBPJ*^{-/-} or *RBPJ*^{+/+} BM donor cells at 30wks post-transplant (left), and of *RBPJ*^{-/-} and *RBPJ*^{+/+} recipient mice transplanted with WT donor cells at 8wks after RBPJ deletion in the microenvironment (right). Results are expressed as fold change of % (n=3-10).

(C) Bar graph summarizes average spleen weight from RBPJ$^{-/-}$, RBPJ$^{+/+}$, RBPJ$^{-/-}$ and RBPJ$^{+/+}$ recipient mice (n=6-9).

(D) % of CMP and GMP in BM and spleen of *RBPJ$^{-/-}$* and *RBPJ$^{+/+}$* mice (n=8-12). Total CMP and GMP numbers/femur in: (E) WT (CD45.1) recipients transplanted with *RBPJ$^{-/-}$* or *RBPJ$^{+/+}$* BM cells; 30wks post-transplant (n=3-5) or (F) *RBPJ$^{-/-}$* and *RBPJ$^{+/+}$* recipients transplanted with WT CD45.1^{+} BM cells; 6-8wks after pIpC (n=6).

(G) Dot Blots indicate Gr1/Mac1 expression in PB, spleen and BM. Bar graphs summarize % of Gr1^{+}/Mac1^{+} cells over whole population; 3 independent experiments (n=6-14).

(H) Neutrophil counts in PB of *RBPJ$^{-/-}$* and *RBPJ$^{+/+}$* mice (left), WT recipients of *RBPJ$^{-/-}$* and *RBPJ$^{+/+}$* donor cells (middle) and of *RBPJ$^{-/-}$* and *RBPJ$^{+/+}$* recipients (right).

(I) Kaplan-Meyer survival curve of *RBPJ$^{-/-}$*, *RBPJ$^{+/-}$*, *RBPJ$^{+/+}$* mice (n=7-14; p<0.01), WT mice recipients of *RBPJ$^{-/-}$* BM cells, and of *RBPJ$^{-/-}$* or *RBPJ$^{+/+}$* mice recipients of WT cells (n=9-11; p<0.01).

All results are shown as mean±SEM; *p<0.05, **p<0.01, ***p<0.005 unless otherwise indicated. See also Figure S1.
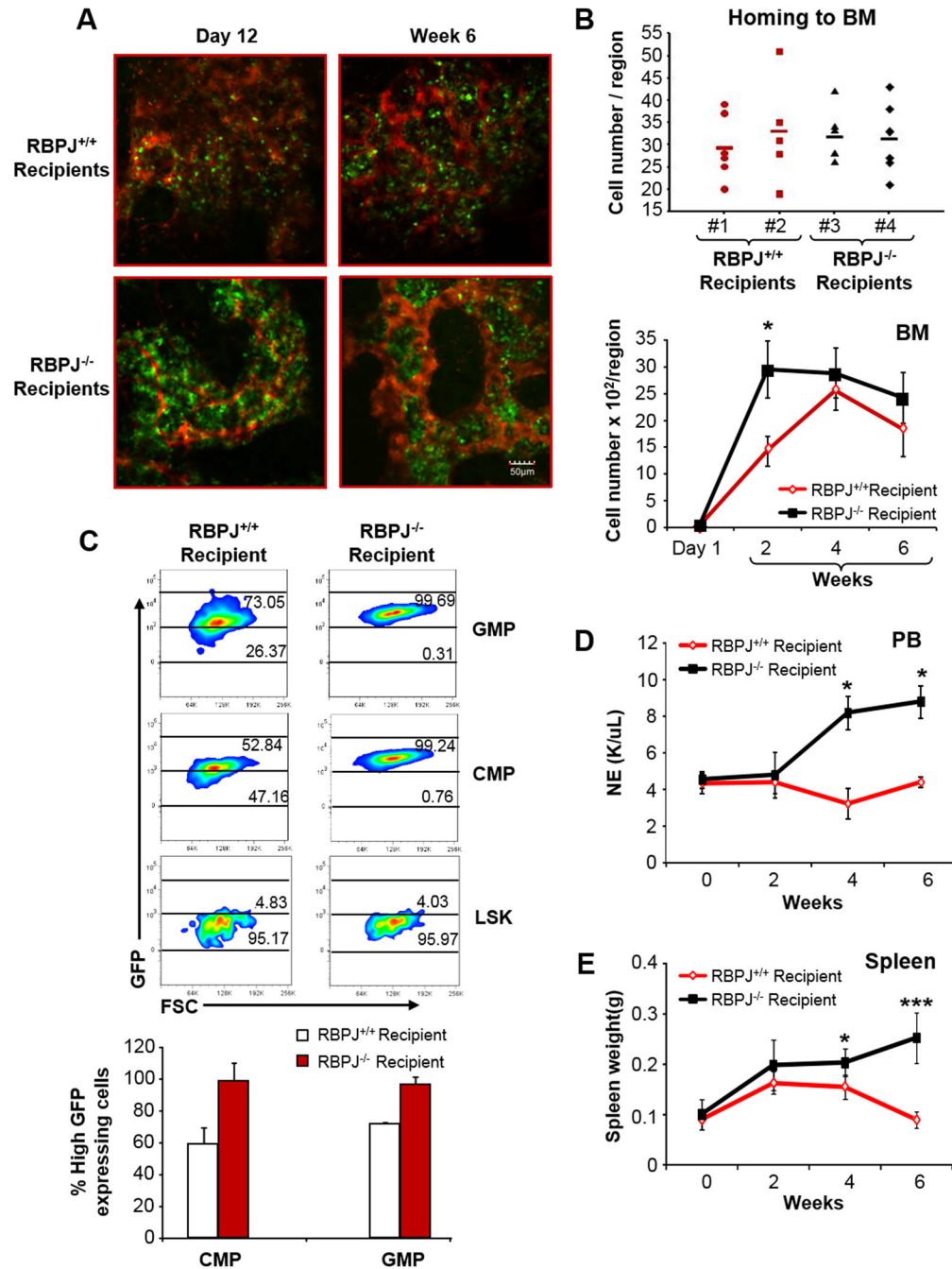
**Figure 2. The *RBPJ*⁻/⁻ BM niche favors myeloid expansion and trafficking**

(A) Intravital imaging of mouse calvarium. *RBPJ*⁻/⁻ mice were induced with pIpC 4wks prior transplantation of BM cells from *Lys-EGFP* donor mice; imaging was performed at 24hrs and wks 2, 4 and 6 post-transplant. Series of 60 μm Z-stacks were collected from 6 regions of calvarium BM in each mouse. Images of 1 representative region of 6 at wks 2 and 6 in *RBPJ*⁻/⁻ and *RBPJ*⁺/⁺ recipients (myeloid cells: green; vasculature; red). Cells were detected automatically and numbers were computed in each region. Scale bar, 50μm.

(B) Upper graph: number of Lys-EGFP$^+$ cells/region homed to BM at 24 hrs: 32±6 cells in *RBPJ*$^{-/-}$ vs. 31 ±8 cells in *RBPJ*$^{+/+}$ recipient mice (n=12 regions; 2 independent experiments; p=NS). Lower graph: kinetics of engraftment of Lys-EGFP cells into *RBPJ*$^{-/-}$ and *RBPJ*$^{+/+}$ recipients over time (mean±SEM of cells in each region; n=12-18 regions; 2-3 mice; *p=0.019).

(C) Lys-EGFP expression on CMP, GMP and LSK at 2wks post-transplant in a representative experiment. Values show % of cells expressing high levels of Lys-EGFP within each specific subset (n=2).

(D) Kinetics of neutrophil mobilization into PB in *RBPJ*$^{-/-}$ and *RBPJ*$^{+/+}$ recipients following transplantation of Lys-EGFP cells into *RBPJ*$^{-/-}$ recipients (mean±SEM; n=4-13; *p<0.005).

(E) Spleen size in *RBPJ*$^{-/-}$ recipients during time following transplantation of Lys-EGFP cells (mean±SD; n=4-6; *p<0.05; ***p<0.005).
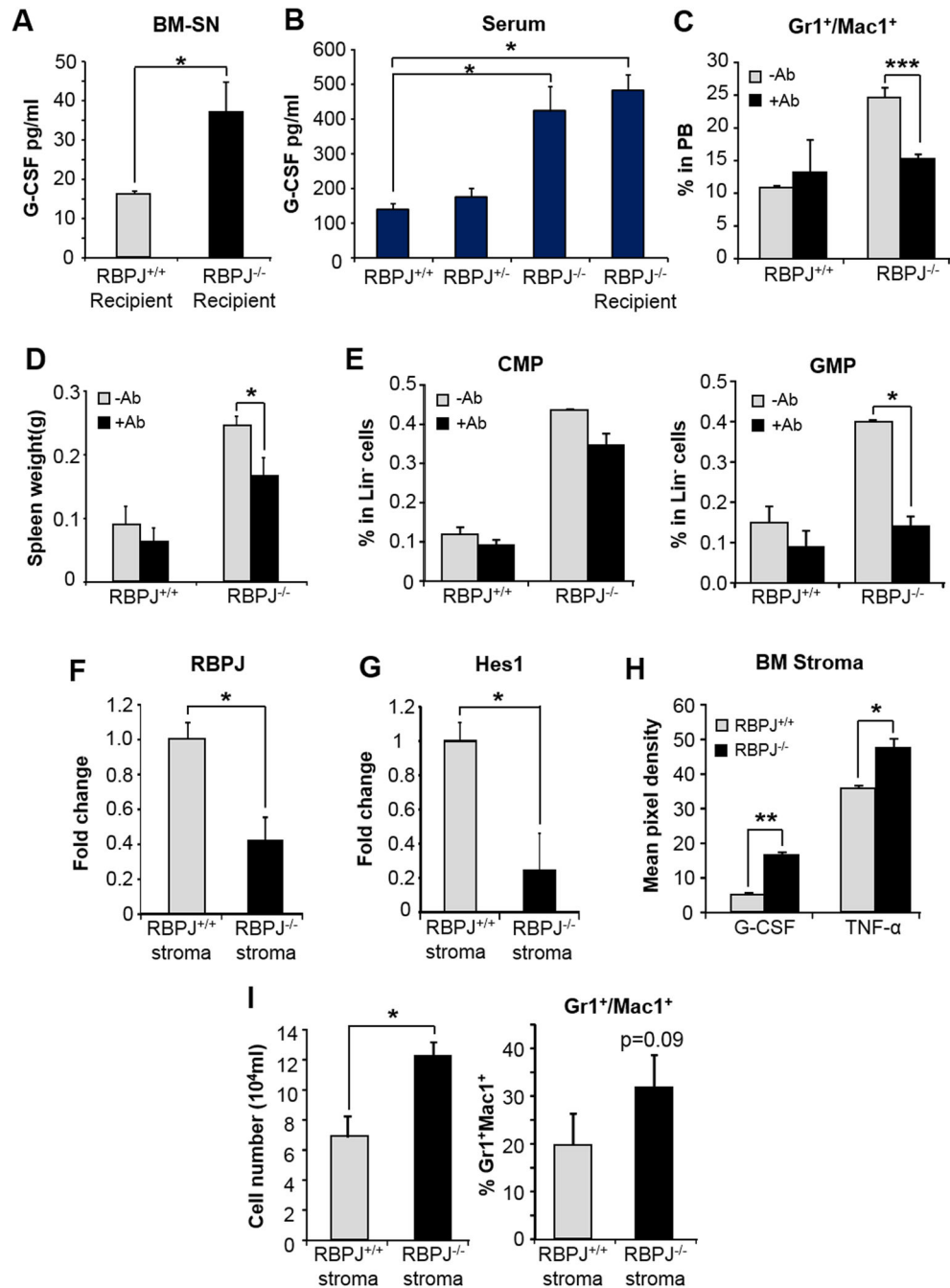
Figure 3. The *RBPJ*$^{-/-}$ BM niche secrets increased levels of G-CSF

(A) G-CSF levels (pg/mL) by ELISA in fresh BM eluted from femurs of *RBPJ*$^{-/-}$ or *RBPJ*$^{+/+}$ recipients 6wks after pIpC induction (n=3).

(B) Serum G-CSF-levels (pg/mL) by ELISA in *RBPJ*$^{+/+}$, *RBPJ*$^{+/-}$, *RBPJ*$^{-/-}$ and *RBPJ*$^{-/-}$ recipient mice 6wks after pIpC induction (n=4).

(C) % of Gr1^{+}/Mac1^{+} cells in PB of *RBPJ*$^{-/-}$ and *RBPJ*$^{+/+}$ mice treated with anti-G-CSF neutralizing Ab or vehicle control (n=3).

(D) Spleens from $RBPJ^{+/+}$ and $RBPJ^{-/-}$ mice treated with G-CSF Ab or vehicle control; representative experiment (n=3).

(E) % of CMP (left) and GMP subsets (right) in spleen of $RBPJ^{-/-}$ and $RBPJ^{+/+}$ mice treated with anti-G-CSF Ab or vehicle control (n=3).

(F) $RBPJ$ and (G) Notch target gene $Hes1$ expression by qRT-PCR in BM stroma from $RBPJ^{-/-}$ or $RBPJ^{+/+}$ mice (n=3).

(H) G-CSF and TNFα levels by cytokine array in BM-derived stroma supernatant from $RBPJ^{-/-}$ and $RBPJ^{+/+}$ mice. Results are expressed as pixel density (n=3).

(I) Left: number of WT Lin⁻ progenitors from 48hrs co-culture on BM stroma from $RBPJ^{-/-}$ or $RBPJ^{+/+}$ mice (n=7). Right: acquisition of myeloid markers by Lin⁻ progenitor cells; results are expressed as % of $Gr1^+/Mac1^+$ cells (n=4; p=0.09).

All results express as mean±SEM; *p<0.05, **p<0.01, ***p<0.005, unless otherwise indicated. See also Figure S2.
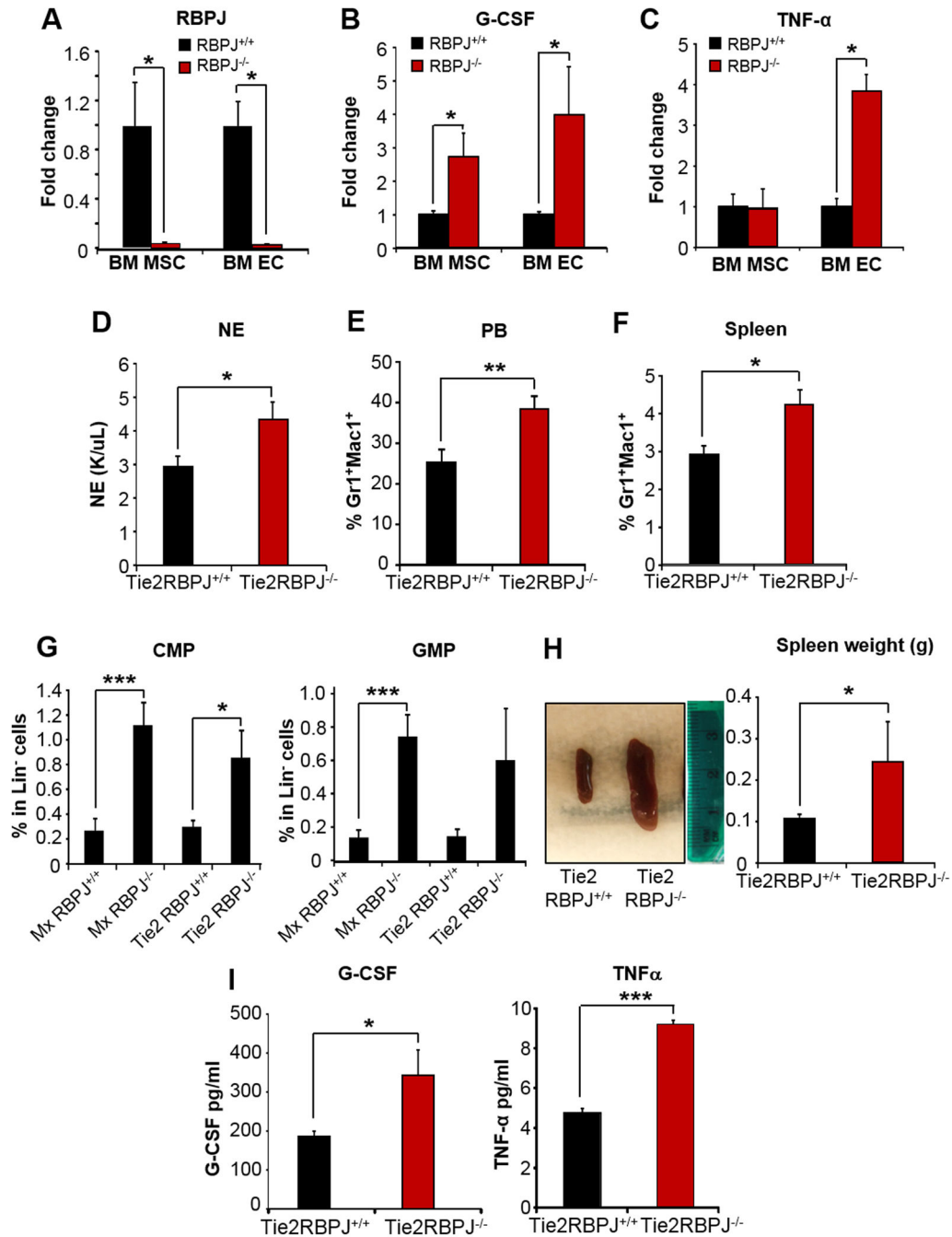
Figure 4. Contribution of the *RBPJ⁻ᐟ⁻* BM endothelial niche to the myeloid expansion
(A) *RBPJ* (B) *G-CSF* and (C) *TNFα* transcript levels by qRT-PCR in sorted
CD45⁻CD105⁺C31⁻ (MSC) and CD45⁻CD105⁺C31⁺ (EC) cells from BM of *RBPJ⁺ᐟ⁺* or
RBPJ⁻ᐟ⁻ mice. Fold change (n=3).
(D) Neutrophil counts and (E) % of Gr1⁺/Mac1⁺ cells in PB (F) % of Gr1⁺/Mac1⁺ cells and
(G) % of CMP and GMP in spleens of *Tie2-RBPJ⁻ᐟ⁻* and *Tie2RBPJ⁺ᐟ⁺* mice at 6 months after
tamoxifen induction compared to *Mx-RBPJ⁻ᐟ⁻* mice induced with pIpC (n=6-7).

(H) Spleens from *Tie2-RBPJ*$^{-/-}$ and *Tie2RBPJ*$^{+/+}$ mice in representative experiment. Bar graph: spleen weights (n=6-7).

(I) G-CSF and TNFα levels (pg/mL) by ELISA in serum of *Tie2-RBPJ*$^{-/-}$ and *Tie2RBPJ*$^{+/+}$ mice 6 months after tamoxifen induction (n=6-7).

All results express as mean±SEM; *p<0.05, **p<0.01, ***p<0.005. See also Figure S3.
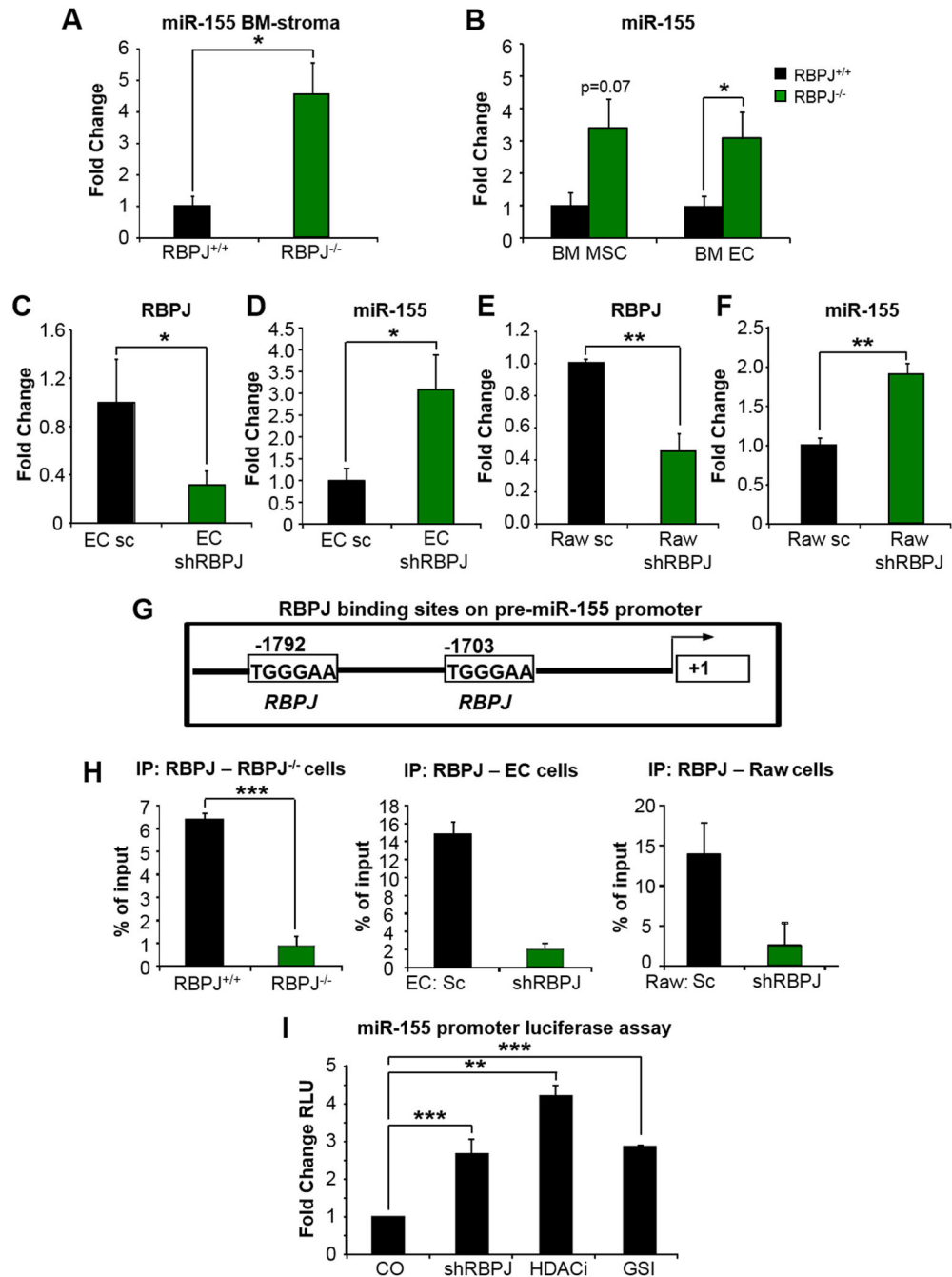
Figure 5. RBPJ functions as repressor on miR-155 promoter

miR-155 levels by qRT-PCR in (A) BM stroma cells from *RBPJ*^{+/+} or *RBPJ*^{-/-} mice (n=4) and (B) BM sorted CD45^{-}CD105^{+}C31^{-} (MSC) or CD45^{-}CD105^{+}C31^{+} (BM EC) cells from *RBPJ*^{+/+}, *RBPJ*^{-/-} mice (n=3); CD45^{-}CD105^{+}C31^{+} cells (n=6) include also BM cells sorted from *Tie2Cre*^{+}*RBPJ*^{-/-} and *Tie2Cre*^{+}*RBPJ*^{+/+} mice. Fold change.

(C) *RBPJ* and (D) *miR-155* transcripts levels by qRT-PCR in EC cells treated with shRBPJ. Fold change (mean±SD; n=2-3).

(E) *RBPJ* and (F) *miR-155* transcripts levels by qRT-PCR in Raw cells treated with shRBPJ. Fold change (n=3).

(G) Scheme of the RBPJ binding sites in the *pre-miR-155/BIC* promoter.

(H) ChIP assay of total BM from $RBPJ^{-/-}$ or $RBPJ^{+/+}$ mice and EC and Raw cells transfected with shRBPJ or scrambled shRNA. IP were conducted with no Ab, an irrelevant Ab, or Abs directed to RBPJ, followed by PCR of the *miR-155* promoter. 3 independent experiments/ each.

(I) miR-155 luciferase assay. Raw cells expressing the *shRBPJ* or treated with HDAC inhibitor (1μM) or with GSI (1μM) were transfected with the *miR-155* promoter region containing the RBPJ binding sites. Results are expressed as fold change in RLU (n=4; 2 independent experiments).

All results express as mean±SEM; *p<0.05, **p<0.01, ***p<0.005. See also Figure S4.
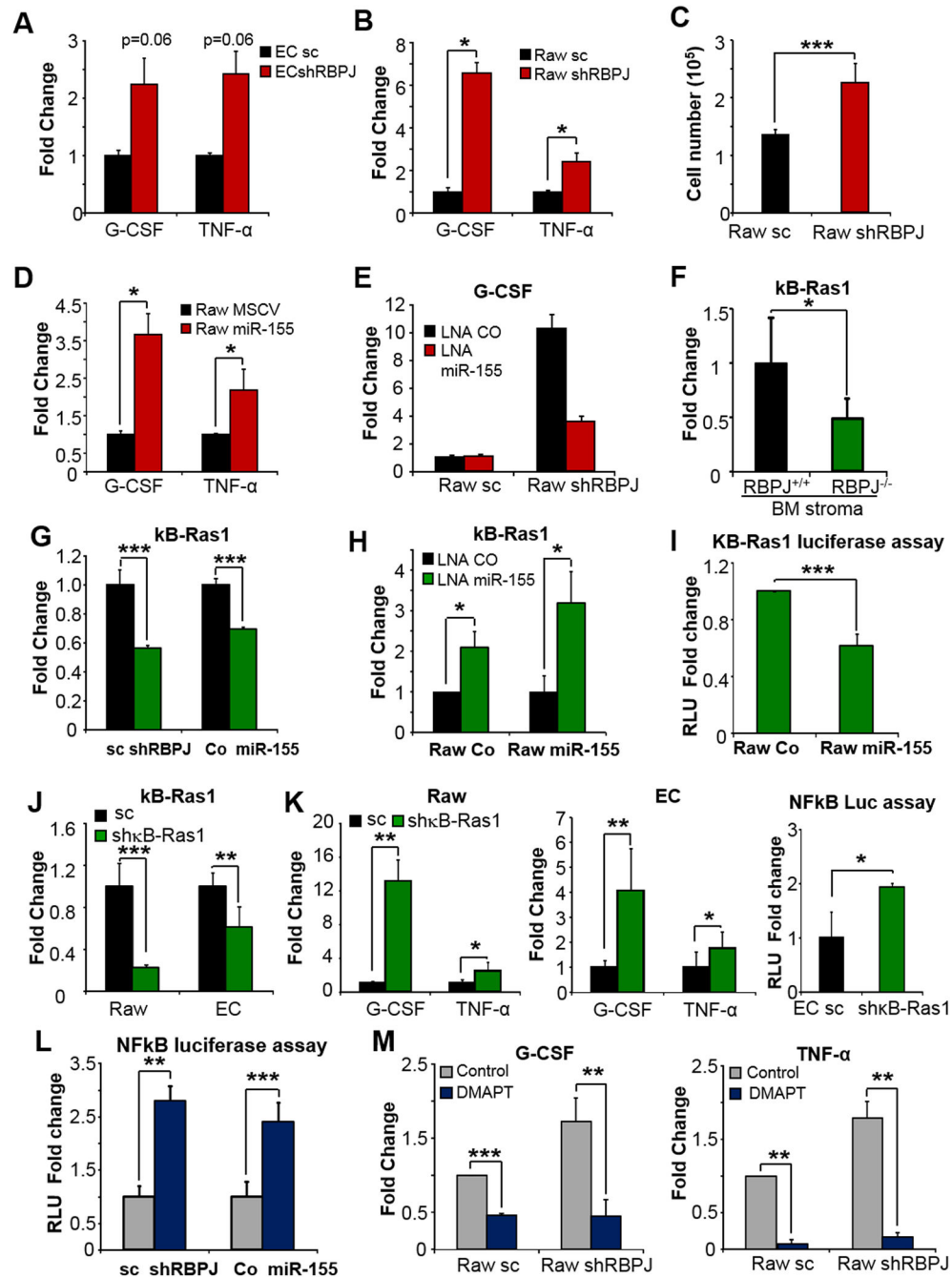
Figure 6. Inhibition of κB-Ras1 by miR-155 upregulates G-CSF and TNFα via NF-κB

(A) EC cells and (B) Raw cells transfected with *shRBPJ* or scrambled shRNA (sc) were analyzed for *G-CSF* and *TNFα* expression by qRT-PCR. Fold change (n=3-5).

(C) Total number WT BM Lin⁻ progenitors co-cultured for 48 hrs with Raw cells transduced with shRBPJ or scrambled shRNA (n=4-6).

(D) *G-CSF* and *TNFα* transcript levels by qRT-PCR in Raw cells transduced with MSCV/GFP or MSCV-miR-155/GFP. Fold change (n=5).

(E) *G-CSF* transcript levels by qRT-PCR in Raw cells transfected with *shRBPJ* and or scrambled shRNA, in the presence of 75nM LNA control or LNA anti-miR155. Representative experiment express in fold change. *κB-Ras1* transcript levels by qRT-PCR in: (F) BM stroma cells from *RBPJ*$^{+/+}$ or *RBPJ*$^{-/-}$ mice. Fold change (n=4), (G) Raw cells transfected with *shRBPJ* and or scrambled shRNA (sc) or transduced with MSCV/GFP (Co) or MSCV-miR-155/GFP (miR155). Fold change (n=4-6), and (H) Raw cells controls (Co) or transduced with MSCV-miR-155/GFP (miR155) in the presence of 75nM LNA control or LNA anti-miR-155 (n=3-6).

(I) *κB-Ras1* 3′UTR Luciferase assay in Raw cells transduced with MSCV/GFP or MSCV-miR-155/GFP. Fold change RLU (n=3).

(J) *κB-Ras1* transcript levels by qRT-PCR in Raw and EC cells transfected with *shκB-Ras1* or scrambled shRNA. Fold change (n=3-4).

(K) Raw and EC cells transfected with *shκB-Ras1* or scrambled shRNA were analyzed for *G-CSF* and *TNFα* expression by qRT-PCR. NFκB Luciferase assay (right panel) in EC cells transfected with *shκB-Ras1* or scrambled shRNA. Fold change (n=3-4).

(L) NFkB Luciferase assay in Raw cells transfected with *shRBPJ* and or scrambled shRNA (sc) or transduced with MSCV/GFP (Co) or MSCV-miR155/GFP. Fold change RLU (n=4-6).

(M) *G-CSF* and *TNFα* transcripts by qRT-PCR in Raw cells transfected with shRBPJ or scrambled shRNA (sc), in culture for 24 hrs with or without 5μM NFkB inhibitor DAMPT. Fold change (n=3).

All results express as mean±SD; *p<0.05, **p<0.01, ***p<0.005. See also Figure S5.
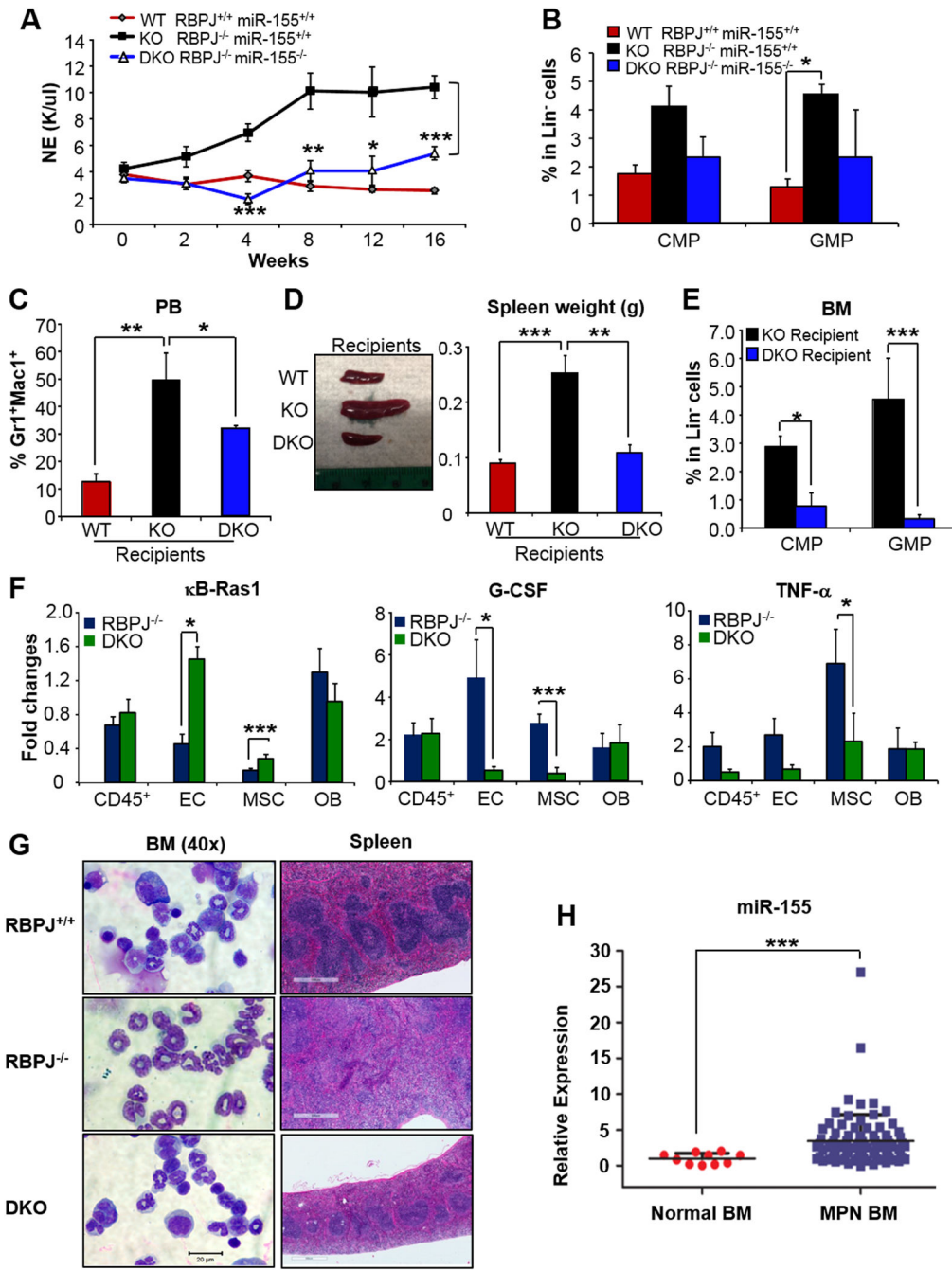
Figure 7. Loss of miR-155 rescues the RBPJ⁻/⁻ phenotype

(A) Neutrophil counts in PB of *RBPJ⁺/⁺miR-155⁺/⁺*, *RBPJ⁻/⁻miR-155⁺/⁺* (KO) and *RBPJ⁻/⁻ miR-155⁻/⁻* (DKO) mice up to 16wks from pIpC induction (n=3-8).

(B) % of BM CMP and GMP subsets in the Lin- population of *RBPJ⁺/⁺miR-155⁺/⁺*, *RBPJ⁻/⁻miR-155⁺/⁺* (KO) and *RBPJ⁻/⁻ miR-155⁻/⁻* (DKO) mice at 20wks after induction (mean±SD; n= 3-8).

(C-E) *RBPJ*^{+/+}*miR-155*^{+/+}, *RBPJ*^{-/-}*miR-155*^{+/+} (KO) and *RBPJ*^{-/-}*miR-155*^{-/-} (DKO) were induced with pIpC and after 2 weeks were transplanted with WT BM cells. At week 10 post-transplant, when level of engraftment was > 90%, data were collected:

(C) % of Gr1^{+}/Mac1^{+} in PB; (mean±SD; n= 3-7).

(D) Representative spleens. Bar graph indicates spleen weight (n=3-6).

(E) % of CMP and GMP in the BM (mean±SD; n= 3-8).

(F) *κB-Ras1, G-CSF* and *TNFα* expression by qRT-PCR in sorted BM CD45^{+}, EC, MSC and cultured OB cells from *RBPJ*^{-/-} and DKO mice. Fold change (n=3-6).

(G) Wright/Gimsa staining of BM cytospins and histological (H&E) analyses of spleen. Scale bar for BM cytospin, 20μm. Scale bar for spleen, 500μm.

(H) *miR-155* expression by qRT-PCR in MPN patients. Dot scatter plot indicates relative expression of *miR-155* in the BM of 85 MF patients and 10 age-matched healthy donors. All results express as mean±SEM; $*p<0.05$, $**p<0.01$, $***p<0.005$, unless otherwise indicated. See also Figure S6.